PROCEEDINGS OF SCIENCE

Search for a heavy neutrino and right-handed W of the left-right symmetric model in pp collisions with the CMS detector

M. Kirsanov[*†]
INR Moscow
E-mail: Mikhail.Kirsanov@cern.ch

We search for signals from the production of right-handed W_R bosons and heavy neutrinos N_l ($l = e, \mu$), that arise naturally in the left-right symmetric extensions to the Standard Model. The search is performed with the CMS Experiment at the LHC using the pp collision data collected in 2011 and 2012 at the 7 and 8 TeV collision energies, correspondingly. The data collected in 2011 correspond to an integrated luminosity of 5 fb^{-1}. The 2012 data used in this analysis correspond to an integrated luminosity of 3.6 fb^{-1}. No excess over expectations from Standard Model processes is observed. For models with the same coupling in the left and right sectors, we exclude the regions in the two-dimensional parameter space that extends up to (M_{W_R}, M_{N_l}) = (2900 GeV, 800 GeV).

LHC on the March - IHEP-LHC,
20-22 November 2012
Institute for High Energy Physics, Protvino,Moscow region, Russia

[*]Speaker.
[†]On behalf of the CMS Collaboration

PoS(IHEP-LHC)039

1. Introduction

The left-right (LR) symmetric extension to the Standard Model model [1, 2, 3] is attractive because it naturally explains the parity violation seen in weak interactions as a result of spontaneously broken parity. The model necessarily incorporates additional $W_R^{\pm}$ and Z' gauge bosons and heavy right-handed neutrino states N_ℓ and thus can also explain the smallness of the ordinary neutrino masses through the see-saw mechanism [4]. In this paper we present the results of the search for heavy neutrinos and the associated heavy gauge bosons of the minimal LR symmetric model using the Compact Muon Solenoid (CMS) detector at the LHC.

The strength of gauge interactions of $W_R^{\pm}$ bosons is described by the coupling constants g_R. Strict LR symmetry leads to the relation $g_L = g_R$ at M_{W_R}, which will be assumed throughout this paper. To simplify our study, we further assume that the mixing angles ($W_R - W_L$, $Z' - Z$, and $N_\ell - N_{\ell'}$) are small. The existing direct experimental limit on the W_R mass from the Tevatron $W_R \to qq$ analysis is in the range 739 - 768 GeV depending on the heavy neutrino mass [5], from the Tevatron $W_R \to tb$ analysis 890 GeV [6] [7]. The direct experimental limit on the W_R mass from the LHC $W_R \to tb$ analysisis is 1.85 TeV [8] [9]. The indirect model-dependent estimates based on the the $K_L - K_S$ mixing results give a limit on the W_R mass of about 2.5 TeV [10], [11].

2. Heavy neutrino production and decay

We consider the leading production reaction at the LHC: $pp \to W_R + X \to N_\ell + \ell + X$. The right-handed neutrino decays into a charged lepton $\ell^{\pm}$ and an off-shell W_R^* which subsequently decays into a pair of quarks which hadronize into jets (j). This produces the final state

$$W_R \to \ell_1 N_\ell \to \ell_1 \ell_2 W_R^* \to \ell_1 \ell_2 jj \quad (\ell = e, \mu), \tag{2.1}$$

where ℓ_1, ℓ_2 have the same flavor. A unique feature of the heavy neutrino production and decay process is that it has a two-dimensional resonance structure. The distributions of the variables $M_{\ell\ell jj}$ and $M_{\ell_2 jj}$ should exhibit rather narrow peaks, with the reconstructed width of $\mathcal{O}(100\ GeV)$ for the W_R mass peak and $\mathcal{O}(50\ GeV)$ for the width of the N_ℓ mass peak. In this analysis, we assume that only one type of heavy neutrino, predominantly coupled to either the electron or muon flavor, will be accessible at LHC energies with the other N_ℓ masses too heavy to produce. However, the case with degenerate N_ℓ masses does not differ significantly, as the opening of an additional decay channel for the W_R would decrease not only the lepton channels but also the quark channels.

Our search is characterized by the W_R and N_ℓ masses, which are allowed to vary independently. We note that the reaction used in the analysis can also proceed if $M_{N_\ell} > M_{W_R}$, but we neglect this possibility due to the relatively small cross section when compared to the dominant production mechanism.

Since QCD does not distinguish between left- and right-handed particles, the k-factor calculation is similar to the W and W' production k-factors [12]. In these calculations, made with the FEWZ program [13], α_s is taken at the W_R mass which results in a k-factor that slowly decreases as a function of M_{W_R}, from 1.33 at $M_{W_R} = 500$ GeV to 1.25 at $M_{W_R} = 2.5$ TeV (can be approximated by a straight line in this range).

We use PYTHIA [15], with default CTEQ6L1 parton distribution functions [16], for the signal event generation and calculation of cross sections. PYTHIA 6.4 includes the LR symmetric model with the standard assumptions mentioned above [17]. We also study relevant background samples generated using PYTHIA (dibosons), NLO generator POWHEG [18] ($t\bar{t}$, tW), SHERPA [19] (Z+jets), MADGRAPH [20] (W+jets).

3. Physical objects reconstruction and event selection

In this analysis we primarily reconstruct electrons, muons and jets, although we also examine photons and the missing transverse energy in the event for selected background studies. We collect the events used in this analysis through double electron trigger and single muon trigger with thresholds that depend on the instantaneous luminosity. For the background studies we also use events collected through single photon trigger. This analysis includes data from 2011, extended by the portion of the 2012 dataset.

We reconstruct electron candidates offline starting by associating electromagnetic clusters in the ECAL with transverse energy $E_T > 40$ GeV with a track in the tracker and apply standard identification and isolation criteria optimized for electrons with energies of hundreds of GeV. The ECAL cluster for each electron candidate must be spatially matched to a reconstructed track in the central tracking system in both η and ϕ. Electron candidates must deposit most of its energy in the ECAL and relatively little in the HCAL, and also have a shower shape consistent with that of an electromagnetic shower. The electron candidate cluster should be isolated from other energy deposits in the calorimeter and from reconstructed tracks in the central tracking system. More information about electron reconstruction and identification in CMS during this running period can be found in [21].

The muon identification strategy is based on both the muon detectors and the inner tracker, as described in [22]. We require $p_T > 40$ GeV/c for both muons. At least one of the muons used to define the WR candidate must be matched to the muon trigger object used to select the events online. Each muon must satisfy identification criteria optimized for muons with large transverse momentum. Muon identification requirements ensure good consistency between the measurements of the muon detector and the inner tracker and suppress muons from decay-in-flight of hadrons as well as shower punch-through. We suppress non-isolated muon backgrounds by summing the transverse momentum of tracks within $\Delta R < 0.3$ of the muon direction and requiring that the final p_T sum, ignoring the muon itself, is less than 10% of the muon p_T.

Jets are reconstructed by forming clusters of charged and neutral hadrons, photons, and leptons that are first reconstructed using the CMS particle-flow technique [23], using the anti-kT clustering algorithm [24] with a cone size parameter $R = 0.5$. Adjusting for the effects of the additional ("pileup") pp collisions in the event, charged hadrons which do not originate from the highest pT primary vertex in the event are ignored during jet clustering. The neutral pileup component is removed by applying a residual area-based correction described in [25], [26]. We impose a minimum transverse momentum requirement of 40 GeV/c on the jet candidates. We apply standard jet identification procedures to suppress jets from calorimeter noise and beam halo, and we reject the event if either of the two highest p_T jet candidates fails identification criteria. The energy of reconstructed jets is corrected based on the results of simulation and data studies [27]. In the

electron channel, and also in studies using $e\mu jj$ events, we do not consider jets if a valid electron candidate is found within the jet radius. As muons are not likely to fake jet signatures, we reject any muon found with $\Delta R(\mu, j) < 0.5$.

We rank the muons and jets in the event according to their transverse momentum and order the electrons according to their transverse energy, where the unique treatment of electrons reflects the dominant contribution of the ECAL energy to the electron energy/momentum measurement. We then select $W_R \to \ell N_\ell$ candidates using the two highest E_T/p_T same-flavor (e or μ) leptons, and the two highest p_T jets that satisfy the above criteria. As the $W_R \to \ell N_\ell$ decay tends to produce high momentum leptons, we further require $E_T(p_T) > 60$ GeV$(/c)$ for at least one of the lepton candidates. In the electron channel, we reject the event if no electron candidate is found in the ECAL barrel region ($|\eta| < 1.44$).

We limit contributions from Standard Model backgrounds by imposing requirements on the dilepton mass ($M_{\ell\ell}$) and the mass of the reconstructed W_R candidate ($M_{\ell\ell jj}$). Electroweak backgrounds, primarily from Z+jets, are suppressed by requiring $M_{\ell\ell}$ be above the Z mass. We find that the optimal cut on $M_{\ell\ell}$ is 200 GeV.

Provided the W_R candidate event meets all acceptance requirements, the ability to reconstruct four high p_T objects using the CMS detector is quite high. Reconstruction efficiency, including the trigger and lepton identification requirements, ranges between 75-80% in the muon channel, and 70-75% in the electron channel.

4. Backgrounds

The background for $W_R \to \ell N_\ell$ decay primarily consists of events from Standard Model processes with two real leptons, such as $t\bar{t}$and Z+jets. It is also possible for jets to be misidentified as leptons, which allows QCD multijet processes to contribute background events.

We estimate the $t\bar{t}$contribution using simulated events, normalizing it to the cross section measured by CMS [28]. We cross check this normalization using a sample of reconstructed $e\mu jj$ events in data and simulation. Based on the results of this study, we apply a scale factor (close to 1) in addition to the cross-section normalization in order to account for the expected top background.

Our estimate of the Z+jets background contribution is based on observation of $Z \to ee, \mu\mu$ decays in simulation and data. We normalize the Z+jets contribution to the inclusive NNLO calculation [12, 13], and then rescale the expected distribution to data (accounting for background contributions) using the reconstructed dilepton mass region near the Z peak in the events with at least two jets. We take the remaining electroweak and top background estimates directly from simulation, as their small cross sections severely limit their impact on the background level.

We determine the QCD multijet background from data using an estimate of the lepton fake rate. For each channel, we examine a sample of dijet events in data in order to determine the lepton fake rate. For the electron channel this sample is selected using photon triggers (prescaled for low E_T photons). Each event should contain at least one electron-like object, i.e. an ECAL cluster satisfying soft shape criteria matched to a track. For the muon channel we collect dijet events using the nominal analysis triggers. We increase the dijet sample purity by rejecting events with missing transverse energy above 20 GeV. The remaining roughly 30% contribution from electroweak and top (as expected from simulation) are statistically removed via simulated event samples. We then

apply the derived fake rate to a multijet sample selected using nominal triggers to estimate the multijet background contribution to the $M_{\ell\ell jj}$ distribution.

As the statistics in the region of high $eejj$ masses is small, causing big statistical errors, we use an exponential lineshape to describe the background contributions. This is done separately for the three parts of background: $t\bar{t}$, Z+jets and all others.

5. Systematic uncertainties

The dominant systematic uncertainty relating to $W_R \to \ell N_\ell$ production is due to variations in the predicted cross-section for the signal production as a result of the uncertainties in the parton distribution functions (PDFs) of the proton. This uncertainty is determined to be 4-22%, depending on the W_R mass hypothesis, following the PDF4LHC prescriptions [29]. The next leading signal uncertainty is due to the lepton reconstruction and identification uncertainties, which are determined from a collection of $Z \to \ell^+\ell^-$ events from both data and simulation.

The background systematic uncertainty is dominated by the uncertainty on the shape of the $M_{\ell\ell jj}$ background distributions. This uncertainty is determined in each mass bin based on the number of events surviving all selection criteria for each background sample. We use the Gamma distribution to describe the systematic uncertainty due to the background shape for each background type, as only a small number of events from simulation and data control samples appear in each mass bin. Log-normal distributions are used for the remaining systematic uncertainties. For the background shape systematic uncertainty, we treat each bin as uncorrelated. All other systematic uncertainties are correlated across $M_{\ell\ell jj}$ bins.

The normalization of the various background samples and additional factorization and scale theoretical uncertainties also contribute to the total systematic uncertainty to a lesser extent. The uncertainties on the total number of background events are derived taking into account the relative contribution of all background events after the full event selection, and the correlation of each systematic effect between the background processes. All systematic uncertainties are summarized in Table 1.

6. Results

We present the $M_{\ell\ell jj}$ distribution for events passing all cuts in Figures 1, 2 and 3. We observe no excess beyond expectations from Standard Model processes.

As we find no evidence for $W_R \to \ell N_\ell$ decay, we estimate limits on W_R production using a multi-bin technique based on the RooStats package [30]. We use the reconstructed four-object mass for a shape analysis. The mass is collected in bins of width 200 GeV up to 1600 GeV, with all events with $M_{\ell\ell jj} > 1600$ GeV collected in a single bin. Systematic uncertainties are included as nuisance parameters in the limit calculations.

We use a CL_S limit setting technique [31, 32] to estimate the 95% C.L. excluded region as a function of the W_R cross-section multiplied by the $W_R \to \ell\ell jj$ branching fraction and W_R mass. The (M_{W_R}, M_{N_ℓ}) limits are obtained by comparing the observed (expected) upper limit and the expected cross section for each mass point. They are presented in Figures 4, 5. The limits extend to roughly

Table 1: Summary of the systematic uncertainties, where each magnitude of uncertainty reflects the deviation from the nominal $M_{\ell\ell jj}$ distribution following the procedures described in the text. The total errors in the bottom row are obtained by summing in quadrature all the relative uncertainties in a given column. The background shape uncertainties are computed in $M_{\ell\ell jj}$ bins, the numbers shown in this table are the weighted average values. The remaining uncertainties are constant as a function of $M_{\ell\ell jj}$. Some uncertainties differ for 2011 and 2012 data, in this case a range is specified. Some uncertainties for the signal, for example PDF, are very different for different mass points, this is the main reason to specify a range in this case. The uncertainties on the total number of background events are derived taking into account the relative contribution of all background events after the full event selection, and the correlation of each systematic effect between the all background processes.

Electron Channel

Systematic Uncertainty	Signal eff.	$t\bar{t}$	Z+jets	QCD	Other bkgd
Jet Energy Scale	±0.1-1%	–	±3%	–	±2%
Jet Energy Resolution	±0.1-1%	–	±1%	–	±1%
Electron Energy Scale	±0.1-1%	–	±0.3%	–	±2%
Electron Reco/ID/Iso	±9-17%	–	±0.1%	–	±9%
Trigger Efficiency	±1-2%	–	±0.2%	–	±1%
Background shape	–	±16-20%	±16-53%	–	±25-35%
Simulation statistics	±2%	–	–	–	–
Background normalization	–	±15%	±3%	–	±4%
PDF	±4-22%	–	±0.4%	–	±9%
Fact./Ren. scale, ISR/FSR	±1-2%	–	±5%	–	±8%
QCD estimate	–	–	–	±33-50%	–
Total	±10-25%	±22%	±21-53%	±33-50%	±34-38%

Muon Channel

Systematic Uncertainty	Signal eff.	$t\bar{t}$	Z+jets	QCD	Other bkgd
Jet Energy Scale	±0.1-1%	–	±2%	–	±2%
Jet Energy Resolution	±0.1-1%	–	±1%	–	±1%
Muon Energy Scale	±0.1-0.5%	–	±2%	–	±1%
Muon Reco/ID/Iso	±6-18%	–	±0.1%	–	±6%
Trigger Efficiency	±0.1-0.3%	–	±0.5%	–	±0.1%
Background shape	–	±16%	±11-49%	–	±30-40%
Simulation statistics	±2%	–	–	–	–
Background normalization	–	±9-11%	±3%	–	±4%
PDF	±4-22%	–	±0.4%	–	±9%
Fact./Ren. scale, ISR/FSR	±1-2%	–	±5%	–	±8%
QCD estimate	–	–	–	±50-60%	–
Total	±8-23%	±21%	±14-49%	±50-60%	±33-44%

$M_{W_R} = 2.5$ TeV in each channel and exclude a wide range of heavy neutrino masses for W_R mass assumptions below this maximal value.

We also present limits as a function of W_R mass for a right-handed neutrino with $M_{N_\ell} = \frac{1}{2}M_{W_R}$ in Fig. 6. Good agreement is seen between the observed and expected limits.

The combined limits for the 7 and 8 TeV data for the muon channel are presented in Fig. 7.

7. Conclusions

We have presented a search for right-handed bosons (W_R) and heavy right-handed neutrinos (N_ℓ) of the left-right symmetric extension of the standard model [33], [34], [35]. We used data collected at the LHC at the collision energies of 7 and 8 TeV. The background contribution from the top and electroweak processes is determined from simulated event samples and the expected rates are normalized to data whenever possible. The background from QCD multijet events is estimated from data. The uncertainty for the backgrounds is estimated using data-driven methods. We find that our data samples are in good agreement with expectations from SM processes. We use a CL_S approach to set a limit on the W_R and N_ℓ masses that includes treatment of the systematic uncertainties as nuisance parameters. 7 and 8 TeV data samples separately, we are able to exclude regions in the (M_{W_R}, M_{N_ℓ}) mass space that extend up to $M_{W_R} = 2.5$ TeV for both channels and for 7 and 8 TeV data. Combining $W_R \to \mu N_\mu$ search results conducted on 7 and 8 TeV collision data, we exclude a region in the (M_{W_R}, M_{N_μ}) mass space that extends to $M_{W_R} = 2.9$ TeV.

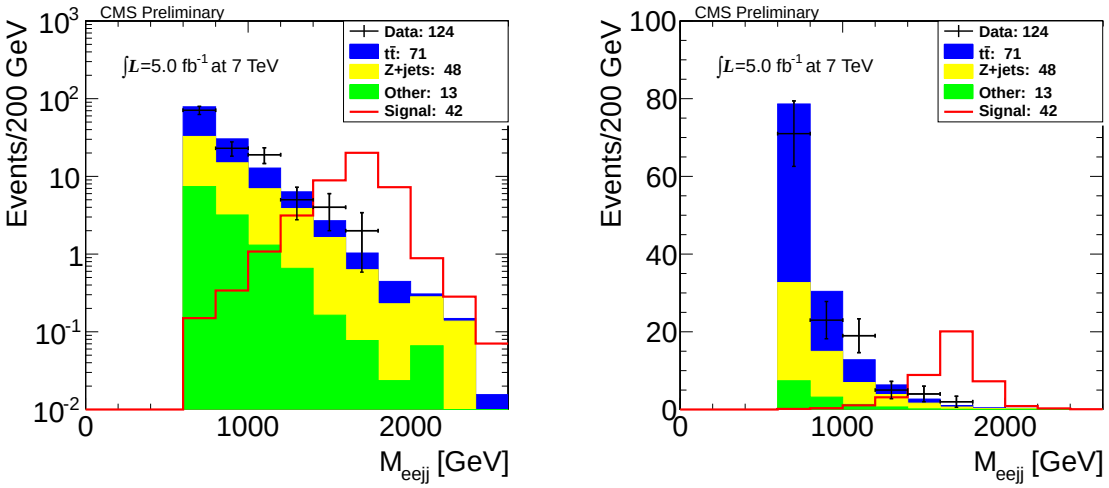

Figure 1: Four-object invariant mass distributions (linear and logarithmic scale plots) for events surviving all selection criteria. The signal mass point $M_{W_R} = 1800$ GeV, $M_{N_e} = 1000$ GeV, is included for comparison.

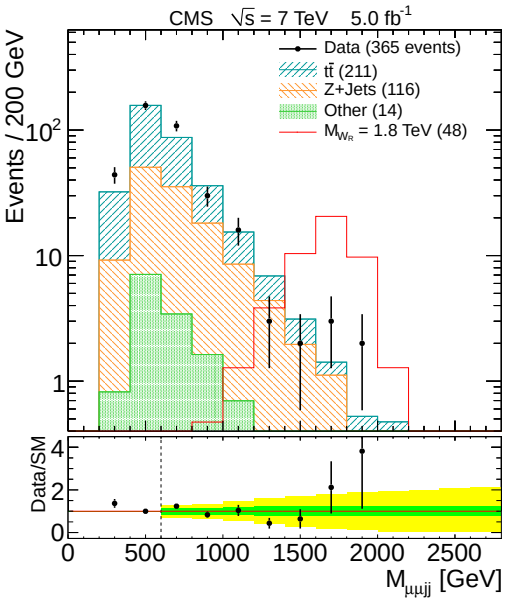

Figure 2: Four-object invariant mass distributions for events surviving all selection criteria. The signal mass point $M_{W_R} = 1800$ GeV, $M_{N_e} = 1000$ GeV, is included for comparison. Green and yellow bands below are the background uncertainties.

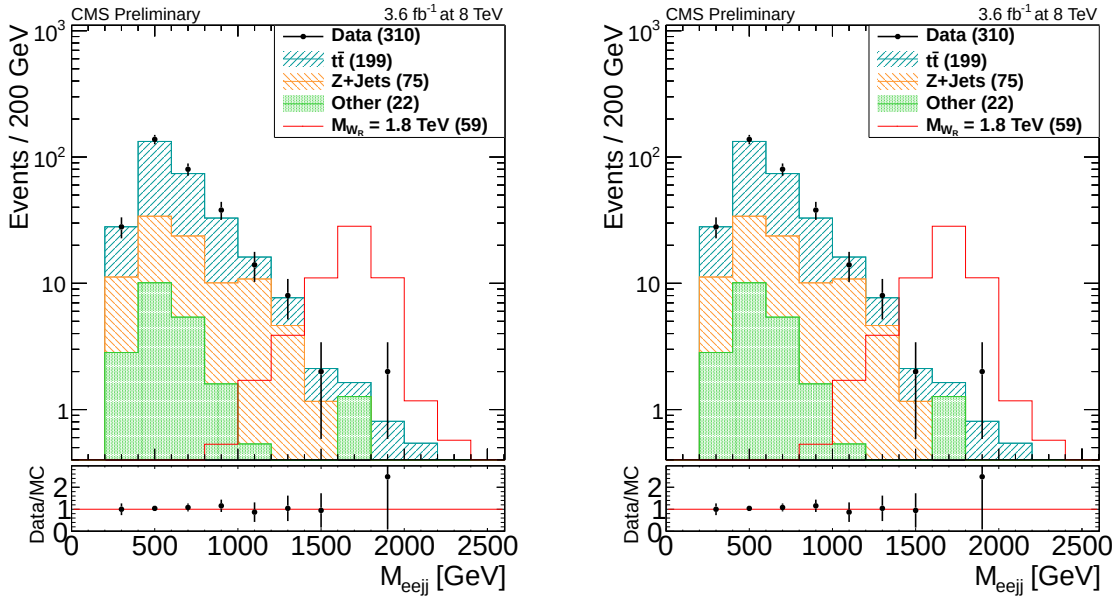

Figure 3: Four-object invariant mass distributions for events surviving all selection criteria. The signal mass point $M_{W_R} = 1800$ GeV, $M_{N_e} = 1000$ GeV, is included for comparison.

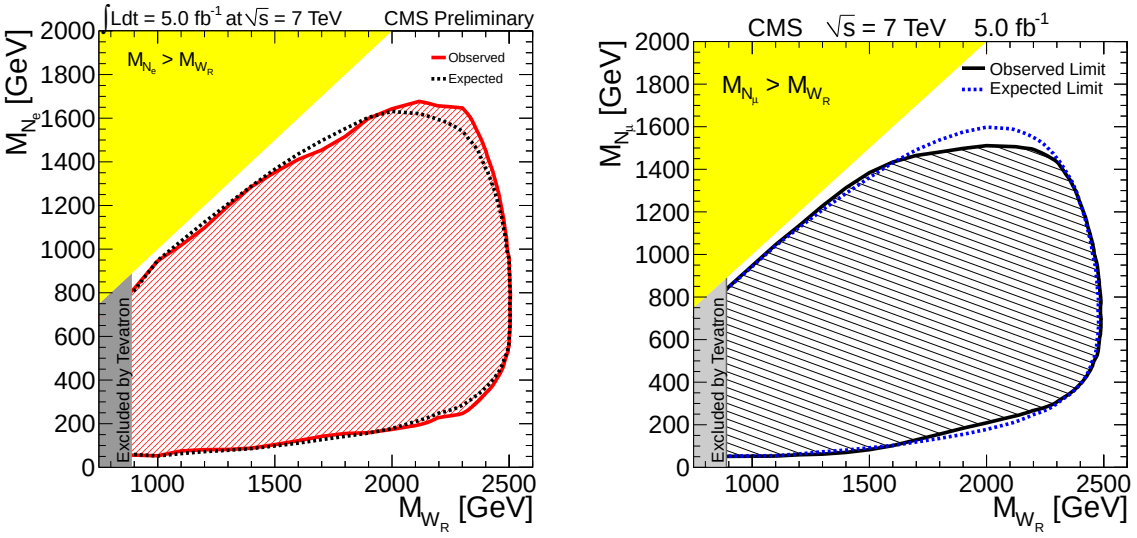

Figure 4: 2D Limits for the 7 TeV LHC data.

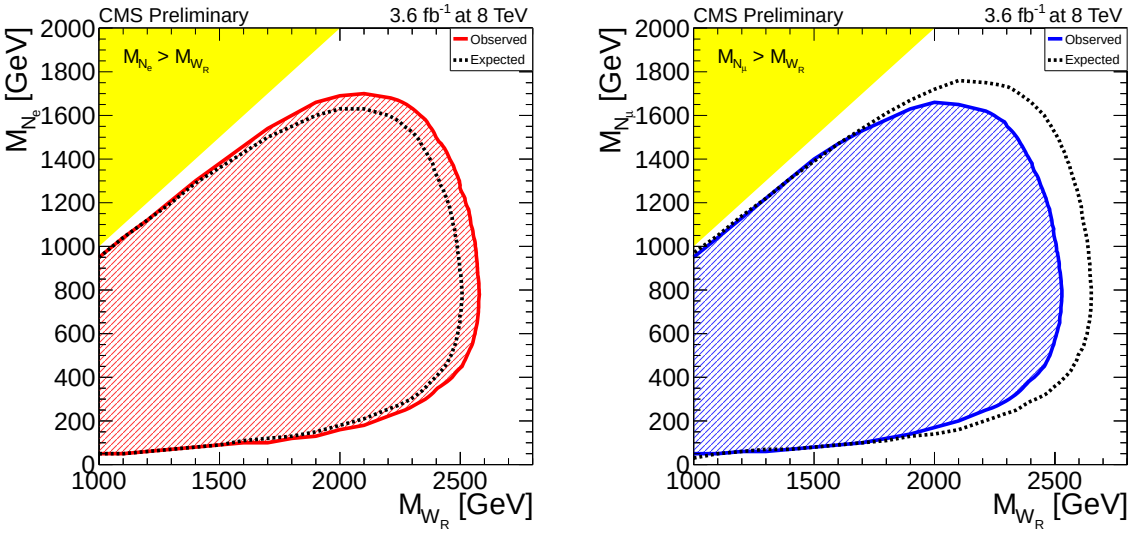

Figure 5: 2D Limits for the LHC data taken at 8 TeV.

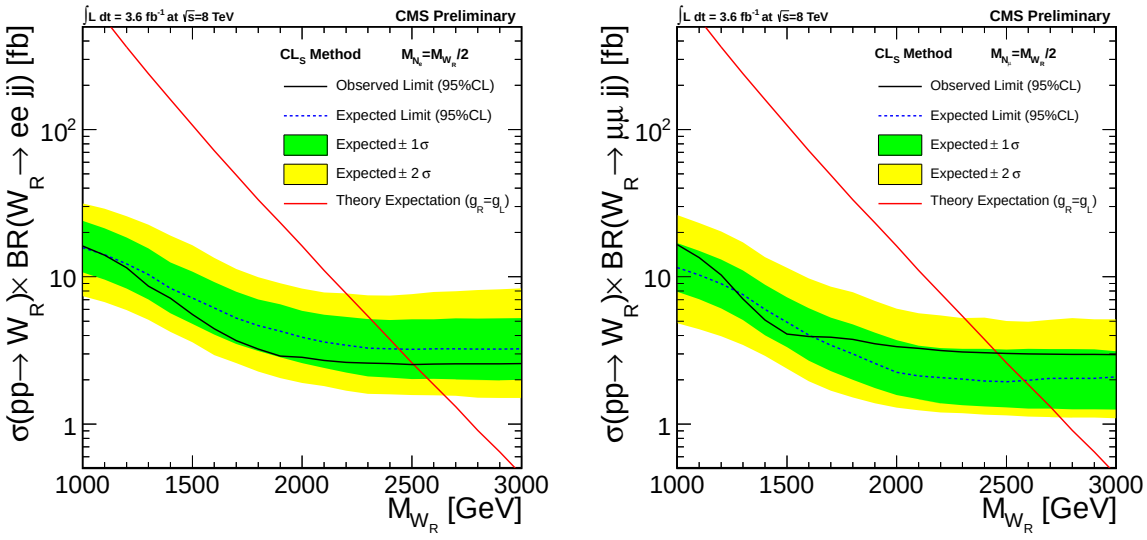

Figure 6: Limits as a function of W_R mass for a right-handed neutrino with $M_{N_\ell} = \frac{1}{2}M_{W_R}$.

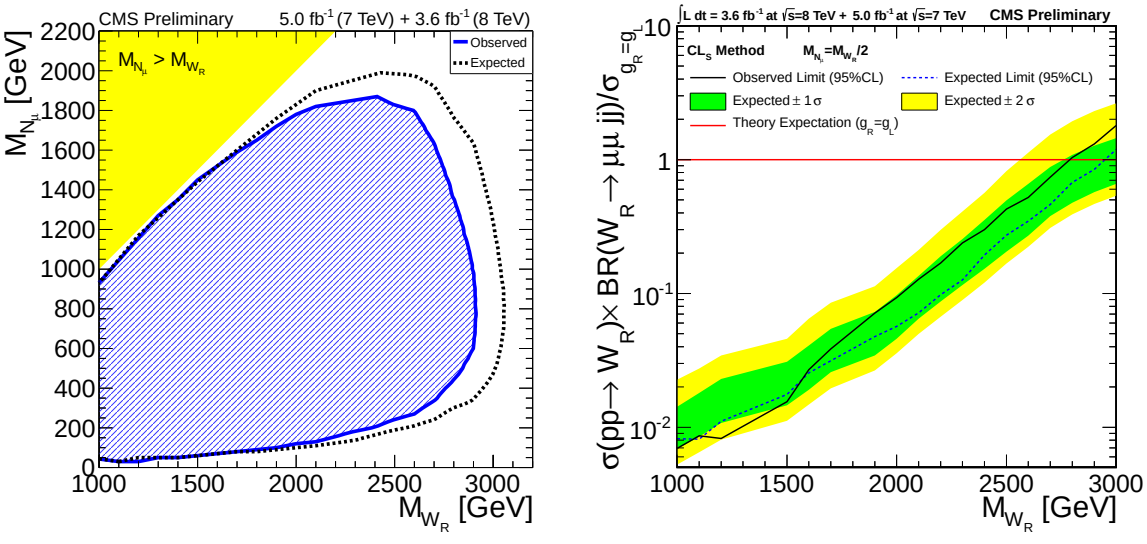

Figure 7: Combined limits for the LHC data taken at 7 and 8 TeV.

References

[1] J. C. Pati and A. Salam *Phys. Rev. D* **10** (1974) 275.

[2] R. N. Mohapatra and J. C. Pati *Phys. Rev. D* **11** (1975) 366.

[3] G.Senjanovic and R.N.Mohapatra *Phys. Rev. D* **12** (1975) 1502.

[4] R. Mohapatra and G. Senjanovic *Phys. Rev. Lett.* **44** (1980) 912.

[5] D0 Collaboration, *Phys. Rev. Lett.* **100** (2008) 211803.

[6] CDF Collaboration, "Search for the Production of Narrow tb Resonancees in 1.9 fb^{-1} of $p\bar{p}$ collisions at 1.96 TeV", *Phys. Rev. Lett.* **103** (2009) 041801.

[7] D0 Collaboration, "Search for $W' \to tb$ resonances with left- and right-handed couplings to fermions", *Phys. Lett. B* **699** (2011) 145.

[8] ATLAS Collaboration, "Search for tb resonances in proton-proton collisions at 7 TeV with the ATLAS detector" (2012), arXiv:1205.1016.

[9] CMS Collaboration, "Search for W' boson decaying to a bottom quark and a top quark in pp collisions at $\sqrt{s}$=7 TeV" (2012), arXiv:1208.0956.

[10] G. Beall, M. Bander, and A. Soni, "Constraint on the Mass Scale of a Left-Right-Symmetric Electroweak Theory from the $K_L - K_S$ Mass Difference", *Phys. Rev. Lett.* **48** (1982) 848.

[11] A. Maiezza, M. Nemevsek, F. Nesti et al., "Left-right symmetry at LHC", *Phys. Rev. D* **82** (2010) 055022.

[12] P.Nadolsky, "Theory of W and Z production", arXiv:hep-ph/0412146.

[13] R. Gavin, Y. Li, F. Petriello et al., "FEWZ 2.0: A code for hadronic Z production at next-to-next-to-leading order", arXiv:1011.3540.

[14] CMS Collaboration *JINST* **3** (2008) S08004.

[15] T.Sjostrand et al. *JHEP* **001-026** (2006), hep-ph/0603175.

[16] J.Botts et al. *Phys. Lett. B* **304** (1993) 159.

[17] G. Bednik and M. Kirsanov, "Comparison of the full matrix element calculation with the simplified calculation of the W_R production at the LHC (left-right symmetric model)", arXiv:1111.6582 [hep-ph].

[18] S. Alioli, P. Nason, C. Oleari et al., "A general framework for implementing NLO calculations in shower Monte Carlo programs: the POWHEG BOX", *JHEP* **1006:043** (2010).

[19] T. Gleisberg et al., "Event generation with SHERPA 1.1", *JHEP* **0902:007** (2009). 0706.2334.

[20] J.Alwall et al., "MadGraph/MadEvent v4: The New Web Generation", *JHEP* **09:028** (2007). 0706.2334.

[21] CMS Collaboration, "Electron reconstruction and identification at $sqrt(s)$=7 TeV", *CMS PAS* **EGM-10-004** (2010).

[22] CMS Collaboration, "Performance of CMS muon identification in pp collisions at $\sqrt{s} = 7TeV$", *CMS PAS* **MUO-2010-002** (2010).

[23] CMS Collaboration, "Commissioning of the Particle-Flow Reconstruction in Minimum-Bias and Jet Events from pp Collisions at 7 TeV", *CMS PAS* **PFT-2010-002** (2010).

[24] M. Cacciari and G. Salam and G. Soyez, “The anti-kt clustering algorithm”, *JHEP* **04** (2008).

[25] M. Cacciari, G. Salam, and G. Soyez, "The Catchment Area of Jets", *JHEP* **04** (2008).

[26] M. Cacciari and G. Salam "Pileup subtraction using jet areas", *Phys. Lett. B* **659** (2008).

[27] CMS Collaboration, "Jet Energy Corrections Determination at 7 TeV", *CMS PAS* **CMS-PAS-JME-10-010** (2010).

[28] CMS Collaboration, "Combination of top quark pair production cross section measurements", *CMS PAS* **CMS-PAS-TOP-11-024** (2011).

[29] PDF4LHCWorking Group, "PDF4LHC Recommendations" (2010).

[30] L. Moneta, K. Belasco, K. Cranmer et al., “The RooStats Project”, *PoS* **ACAT2010** (2010) 057, arXiv:1009.1003.

[31] A. L. Read, "Presentation of search results: the CLstechnique" *J. Phys. G* **28** (2002) 2693.

[32] T. Junk, "Confidence level computation for combining searches with small statistics", *Nucl. Instrum. Meth. A* **434** (1999) 435.

[33] CMS Collaboration, "Search for a heavy electron neutrino N_e and right-handed W bosons of the left-right symmetric model in pp collisions at $\sqrt{s}$=7 TeV", *CMS PAS* **CMS-PAS-EXO-12-004** (2012).

[34] CMS Collaboration, "Search for heavy neutrinos and with right-handed couplings in a left-right symmetric model in at 7 TeV", *Phys. Rev. Lett.* **109** (2012) 261802, CERN Preprint CERN-PH-EP-2012-235, arXiv:1210.2402.

[35] CMS Collaboration, "Search for a heavy neutrino and right-handed W of the left-right symmetric model in pp collisions at $\sqrt{s}$ = 8 TeV", *CMS PAS* **CMS-PAS-EXO-12-017** (2012).